Temperature-Dependent Solvation Dynamics of Water in Sodium Bis(2-ethylhexyl)sulfosuccinate/Isooctane Reverse Micelles

Rajib Kumar Mitra, Sudarson Sekhar Sinha, and Samir Kumar Pal*

Unit for Nano Science and Technology, Department of Chemical, Biological, and Macromolecular Sciences, S.N. Bose National Center for Basic Sciences, Block JD, Sector III, Salt Lake, Kolkata 700098, India

In this paper, for the first time, we report a detailed study of the temperature-dependent solvation dynamics of a probe fluorophore, coumarin-500, in AOT/isooctane reverse micelles (RMs) with varying degrees of hydration (w_0) of 5, 10, and 20 at four different temperatures, 293, 313, 328, and 343 K. The average solvation time constant becomes faster with the increase in w_0 values at a particular temperature. The solvation dynamics of a RM with a fixed w_0 value also becomes faster with the increase in temperature. The observed temperature-induced faster solvation dynamics is associated with a transition of bound- to free-type water molecules, and the corresponding activation energy value for the $w_0 = 5$ system has been found to be 3.4 kcal mol^{-1}, whereas for the latter two systems, it is ∼5 kcal mol^{-1}. Dynamic light scattering measurements indicate an insignificant change in size with temperature for RMs with w_0 = 5 and 10, whereas for a $w_0 = 20$ system, the hydrodynamic diameter increases with temperature. Time-resolved fluorescence anisotropy studies reveal a decrease in the rotational restriction on the probe with increasing temperature for all systems. Wobbling-in-cone analysis of the anisotropy data also supports this finding.

Introduction

Reverse micelles (RMs) provide an attractive model system for biomolecules since they can mimic several important and essential features of biological membranes. One of the most important features of RMs is the presence of highly structured yet heterogeneous water molecules, which represent an interesting model of water molecules present in biological systems such as membranes. The physical and chemical properties of the entrapped water are markedly different from those of bulk water but similar in several aspects to those of biological interfacial water as found in membranes or protein interfaces.[1−4] The key structural parameter of RMs is the molar ratio of water and surfactant (degree of hydration, w_0 = [water]/[surfactant]), which determines the micellar size as well as the unique physicochemical properties of the entrapped water. Thus, RMs are a unique type of molecular assembly that offers the unique advantage of monitoring the dynamics of embedded molecules with varying degrees of hydration.[5,6]

The double tailed anionic surfactant sodium bis(2-ethylhexyl)-sulfosuccinate (AOT) is one of the most extensively investigated surfactants for the study of such heterogeneous systems since it can form spherical RMs in many nonpolar solvents over a wide range of w_0 values.[7,8] The properties of the entrapped water in AOT/RMs have previously been investigated using different techniques.[9−15] A study using FT-IR reveals the existence of four different kinds of water molecules in AOT/isooctane (AOT/i-Oc) RMs, namely, free monomers, dimers at the interface, monomers bonded to the interface, and the bulk-type.[16] The study reveals that with increasing w_0 values, the amount of bulk water increases at the expense of monomer water. After a certain w_0 value, all four types of water molecules remain in constant proportion. However, there are several other studies in the literature[17−22] that question the possibility of such amounts of different kinds of water in the RMs. All these studies show that there is bound water until the polar head of the surfactant and their counterions are completely solvated, after which the water starts to form a bulk-type water pool. While much attention has been paid to the structural features of such systems, relatively less is known about the dynamical properties of the entrapped water. Only a few groups of researchers have so far reported the

* Corresponding author. E-mail: skpal@bose.res.in.
(1) Jain, T. K.; Varshney, M.; Maitra, A. *J. Phys. Chem.* **1989**, *93*, 7409−7416.
(2) Ikushima, Y.; Saito, N.; Arai, M. *J. Colloid Interface Sci.* **1997**, *186*, 254−263.
(3) Venables, D. S.; Huang, K.; Schmuttenmaer, C. A. *J. Phys. Chem. B* **2001**, *105*, 9132−9138.
(4) Brubach, J.-B.; Mermet, A.; Filabozzi, A.; Gerschel, A.; Lairez, D.; Krafft, M. P.; Roy, P. *J. Phys. Chem. B* **2001**, *105*, 430−435.
(5) Luisi, P. L.; Straub, B. E. *Reverse Micelles*; Plenum Press: New York, 1984.
(6) Structure and Reactivity in Reverse Micelles. In *Studies in Physical and Theoretical Chemistry*; Pileni, M. P., Ed.; Elsevier: Amsterdam, 1989; Vol. 65.
(7) De, T. K.; Maitra, A. *Adv. Colloid Interface Sci.* **1995**, *59*, 95−193.
(8) Nave, S.; Eastoe, J.; Heenan, R. K.; Steytler, D.; Grillo, I. *Langmuir* **2000**, *16*, 8741−8748.

(9) D'Aprano, A.; Lizzio, A.; Turco Liveri, V.; Aliotta, F.; Vasi, C.; Migliardo, P. *J. Phys. Chem.* **1988**, *92*, 4436−4439.
(10) Belletête, M.; Lachapelle, M.; Durocher, G. *J. Phys. Chem.* **1990**, *94*, 5337−5341.
(11) Heatley, F. *J. Chem. Soc., Faraday Trans. 1* **1989**, *85*, 917−928.
(12) Goto, A.; Yoshioka, H.; Kishimoto, H.; Fujita, T. *Langmuir* **1992**, *8*, 441−445.
(13) Goto, A.; Harada, S.; Fujita, T.; Miwa, Y.; Yoshioka, H.; Kishimoto, H. *Langmuir* **1993**, *9*, 86−89.
(14) Goto, A.; Yoshioka, H.; Manabe, M.; Goto, R. *Langmuir* **1995**, *11*, 4873−4875.
(15) Zhou, N.; Li, Q.; Wu, J.; Chen, J.; Weng, S.; Xu, G. *Langmuir* **2001**, *17*, 4505−4509.
(16) González-Blanco, C.; Rodríguez, L. J.; Velázquez, M. M. *J. Colloid Interface Sci.* **1999**, *211*, 380−386.
(17) Novaki, L. P.; El Seoud, O. A. *J. Colloid Interface Sci.* **1998**, *202*, 391−398.
(18) Christopher, D. J.; Yarwood, J.; Belton, P. S.; Hills, B. P. *J. Colloid Interface Sci.* **1992**, *152*, 465−472.
(19) Silber, J. J.; Biasutti, A.; Abuin, E.; Lissi, E. *Adv. Colloid Interface Sci.* **1999**, *82*, 189−252.
(20) Novaki, L. P.; Pires, P. A. R.; El Seoud, O. A. *Colloid Polym. Sci.* **2000**, *278*, 143−149.
(21) Piletic, I. R.; Moilanen, D. E.; Spry, D. B.; Levinger, N. E.; Fayer, M. D. *J. Phys. Chem. A* **2006**, *110*, 4985−4999.
(22) Piletic, I. R.; Moilanen, D. E.; Levinger, N. E.; Fayer, M. D. *J. Am. Chem. Soc.* **2006**, *128*, 10366−10367.

solvation dynamics of polar solvents entrapped in RMs.[23−46] The ability of solvent molecules to move in response to a changing electric field has been shown to be important for understanding a range of fast chemical processes.[47] Polar solvation dynamics follow the change in environment following the instantaneous change of a charge distribution of a reporter probe molecule.[48]

The studies made so far using different kinds of RM systems reveal a consistent result that regardless of RM medium and molecular probe, the dynamics appear to be significantly slowed down by the confined environment of the RM.[29,49] As reported by Levinger et al.,[23−25] a dramatic slowing down of the solvation dynamics occurs inside the AOT/RM regardless of the counterion. This group has also reported fast relaxation in several systems, indicating ultrafast bulk water relaxation. For AOT/RM, the amplitude of fast relaxation increases as w_0 increases. For lecithin and nonionic RMs, the fast solvation is more prominent when the RMs have a spherical morphology.[26−28] Corbeil and Levinger's recent report suggests that the solvent reorganization in quaternary microemulsion systems is significantly slower than the ternary RM systems.[38] Bhattacharyya et al.[30−33] have made a significant effort in understanding the solvation dynamics in various RM systems using picosecond-resolved fluorescence spectroscopy. Sarkar et al.[45,46] have studied solvation dynamics of various probes in water-in-oil microemulsions and reverse micelles. Majumder et al.[39] studied the solvation dynamics of coumarin-500 (C-500) in AOT/i-Oc RM with $w_0 = 10$ at room temperature using a picosecond-resolved fluorescence technique. They showed that when excited at $\lambda_{ex} = \sim400$ nm, the probe molecules residing at the AOT/i-Oc polar interface become selectively excited. They observed slow solvation and rotational

relaxation dynamics of the probe. Molecular simulation studies[50−53] reveal that water is largely immobilized at the micellar interface by strong interactions with polar head groups and counterions. Water trapped in this ionic layer at the surfactant surface or bound to the ionic layer shows a decreased mobility. As w_0 increases, a bulk-like water pool is formed in the micellar interior. The bulk-like characteristic appears within a few monolayers of the surfactant surface. The solvation response in RMs becomes faster as w_0 increases.

To the best of our knowledge, no group has ever attempted to study the solvation dynamics of RM as a function of temperature, whereas there are some reports on the effect of temperature on the solvation dynamics of micellar systems.[54−57] This might be due to the fact that the structural integrity of RMs is not assured over this temperature range. It is known that several RM systems are very sensitive toward temperature.[58,59] Depending upon the nature of the oil and water content, the flexibility of the interfacial film changes with temperature. Oils that penetrate deep into the interfacial layer make the film rigid and thus insensitive toward temperature, whereas long chain alkanes that cannot penetrate deep into the interfacial layer make the interface more fluid with increasing temperature at a fixed w_0 value.[60−62] It is not clearly known as to whether this also changes the physicochemical characteristics of the entrapped water. A recent report[63] suggests that the hydrogen bond strength of interfacial water increases as the temperature is lowered. RMs are less susceptible to temperature related perturbation than bulk water. Thus, it is important to understand the nature of the temperature-dependent solvation dynamics of water entrapped in RMs. As a primary step toward an exploration in this arid field, we herein report the solvation dynamics of the probe C-500 in AOT-in-isooctane (i-Oc) RMs with varying degrees of hydration ($w_0 = 5$, 10, and 20) at four different temperatures, 293, 313, 328, and 343 K using a picosecond-resolved TCSPC technique. The choice of w_0 value is justified by the fact that AOT/i-Oc RMs form a well-defined water pool at $w_0 = 10$. At a lower hydration level, the water molecules only hydrate the polar head groups of AOT, and at $w_0 > 10$, the added water goes into the water pool to increase its size. We attempted to study the temperature-dependent solvation dynamics in all these three levels of hydration. The structure of these RMs at different temperatures was determined using the dynamic light scattering (DLS) technique. The choice of the probe is justified due to its unique property that when excited at ~400 nm, the probe molecules residing at the polar interface (water/AOT head group) are selectively excited,[39] and we obtain information solely coming from the interface and its immediate vicinity. Rotational relaxation dynamics of the dye in different RM systems at different

(23) Pant, D.; Riter, R. E.; Levinger, N. E. *J. Chem. Phys.* **1998**, *109*, 9995−10003.
(24) Riter, R. E.; Willard, D. M.; Levinger, N. E. *J. Phys. Chem. B* **1998**, *102*, 2705−2714.
(25) Riter, R. E.; Undiks, E. P.; Levinger, N. E. *J. Am. Chem. Soc.* **1998**, *120*, 6062−6067.
(26) Willard, D. M.; Riter, R. E.; Levinger, N. E. *J. Am. Chem. Soc.* **1998**, *120*, 4151−4160.
(27) Willard, D. M.; Levinger, N. E. *J. Phys. Chem. B* **2000**, *104*, 11075−11080.
(28) Pant, D.; Levinger, N. E. *Langmuir* **2000**, *16*, 10123−10130.
(29) Levinger, N. E. *Curr. Opin. Colloid Interface Sci.* **2000**, *5*, 118−124.
(30) Sarkar, N.; Das, K.; Datta, A.; Das, S.; Bhattacharyya, K. *J. Phys. Chem.* **1996**, *100*, 10523−10527.
(31) Das, S.; Datta, A.; Bhattacharyya, K. *J. Phys. Chem. A* **1997**, *101*, 3299−3304.
(32) Mandal, D.; Datta, A.; Pal, S. K.; Bhattacharyya, K. *J. Phys. Chem. B* **1998**, *102*, 9070−9073.
(33) Pal, S. K.; Mandal, D.; Sukul, D.; Bhattacharyya, K. *Chem. Phys. Lett.* **1999**, *312*, 178−184.
(34) Sen, S.; Dutta, P.; Sukul, D.; Bhattacharyya, K. *J. Phys. Chem. A* **2002**, *106*, 6017−6023.
(35) Dutta, P.; Sen, P.; Mukherjee, S.; Halder, A.; Bhattacharyya, K. *J. Phys. Chem. B* **2003**, *107*, 10815−10822.
(36) Mandal, D.; Sen, S.; Sukul, D.; Bhattacharyya, K.; Mandal, A. K.; Banerjee, R.; Roy, S. *J. Phys. Chem. B* **2002**, *106*, 10741−10747.
(37) Dutt, G. B. *J. Phys. Chem. B* **2004**, *108*, 805−810.
(38) Corbeil, E. M.; Levinger, N. E. *Langmuir* **2003**, *19*, 7264−7270.
(39) Majumder, P.; Sarkar, R.; Shaw, A. K.; Chakraborty, A.; Pal, S. K. *J. Colloid Interface Sci.* **2005**, *290*, 462−474.
(40) Shirota, H.; Segawa, H. *Langmuir* **2004**, *20*, 329−335.
(41) Shirota, H.; Horie, K. *J. Phys. Chem. B* **1999**, *103*, 1437−1443.
(42) Riter, R. E.; Undiks, E. P.; Kimmel, J. R.; Levinger, N. E. *J. Phys. Chem. B* **1998**, *102*, 7931−7938.
(43) Satoh, T.; Okuno, H.; Tominaga, K.; Bhattacharyya, K. *Chem. Lett.* **2004**, *33*, 1090−1092.
(44) Raju, B. B.; Costa, S. M. B. *Phys. Chem. Chem. Phys.* **1999**, *1*, 5029−5034.
(45) Seth, D.; Chakraborty, A.; Setua, P.; Sarkar, N. *Langmuir* **2006**, *22*, 7768−7775.
(46) Seth, D.; Chakraborty, A.; Setua, P.; Sarkar, N. *J. Chem. Phys.* **2007**, *126*, 224512 (1−12).
(47) Stratt, R. M.; Maroncelli, M. *J. Phys. Chem.* **1996**, *100*, 12981−12996.
(48) Horng, M. L.; Gardecki, J. A.; Papazyan, A.; Maroncelli, M. *J. Phys. Chem.* **1995**, *99*, 17311−17337.
(49) Bhattacharyya, K. *Acc. Chem. Res.* **2003**, *36*, 95−101.

(50) Brown, D.; Clarke, J. H. R. *J. Phys. Chem.* **1988**, *92*, 2881−2888.
(51) Linse, P. *J. Chem. Phys.* **1989**, *90*, 4992−5004.
(52) Faeder, J.; Ladanyi, B. M. *J. Phys. Chem. B* **2000**, *104*, 1033−1046.
(53) Faeder, J.; Ladanyi, B. M. *J. Phys. Chem. B* **2001**, *105*, 11148−11158.
(54) Sen, S.; Mukherjee, S.; Halder, A.; Bhattacharyya, K. *Chem. Phys. Lett.* **2004**, *385*, 357−361.
(55) Kumbhakar, M.; Goel, T.; Mukherjee, T.; Pal, H. *J. Phys. Chem. B* **2004**, *108*, 19246−19254.
(56) Kumbhakar, M.; Goel, T.; Nath, S.; Mukherjee, T.; Pal, H. *J. Phys. Chem. B* **2006**, *110*, 25646−25655.
(57) Mitra, R. K.; Sinha, S. S.; Pal, S. K. *J. Phys. Chem. B* **2007**, *111*, 7577−7581.
(58) Mitra, R. K.; Paul, B. K. *Colloids Surf., A* **2005**, *255*, 165−180.
(59) Lang, J.; Mascolo, G.; Zana, R.; Luisi, P. L. *J. Phys. Chem.* **1990**, *94*, 3069−3074.
(60) Hou, M. J.; Shah, D. O. *Langmuir* **1987**, *3*, 1086−1096.
(61) Leung, R.; Shah, D. O. *J. Colloid Interface Sci.* **1987**, *120*, 320−329.
(62) Paul, B. K.; Mitra, R. K. *J. Colloid Interface Sci.* **2005**, *288*, 261−279.
(63) Nucci, N. V.; Vanderkooi, J. M. *J. Phys. Chem. B* **2005**, *109*, 18301−18309.

Scheme 1. Molecular Structure of C-500

H_3CH_2CHN
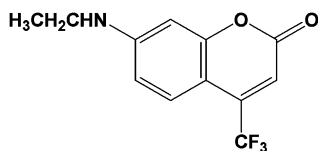
Coumarin 500 (C-500)

temperatures has also been determined by using picosecond-resolved fluorescence anisotropy decay.

Materials and Methods

Sodium bis(2-ethylhexyl)sulfosuccinate (AOT) and isooctane (i-Oc) were products of Sigma and Spectrochem, respectively, and were used without further purification. C-500 (Scheme 1) was obtained from Exciton. AOT was dissolved in isooctane to a concentration of 100 mM, and then the calculated amount of water was injected into it to produce the reverse micelles (RMs) of desired hydration (w_0). Temperature-dependent steady-state absorption and emission were measured with a Shimadzu UV-2450 spectrophotometer and Jobin Yvon Fluoromax-3 fluorimeter, respectively, with temperature controller attachments from Julabo (Model: F32). DLS measurements were performed with a NanoS Malvern instrument employing a 4 mW He−Ne laser ($\lambda = 632.8$ nm) equipped with a thermostated sample chamber. All the scattered photons were collected at a 173° scattering angle. The scattering intensity data were processed using the instrumental software to obtain the hydrodynamic diameter (d_h) and size distribution of the scatterer in each sample. The instrument measures the time-dependent fluctuation in the intensity of light scattered from the particles in solution at a fixed scattering angle. The hydrodynamic diameter (d_h) of the micelles was estimated from the intensity auto-correlation function of the time-dependent fluctuation in intensity. d_h is defined as

$$d_h = \frac{k_b T}{3\pi\eta D} \tag{1}$$

where k_b is the Boltzmann constant, η is the viscosity, and D is the translational diffusion coefficient. In a typical size distribution graph from the DLS measurement, the x-axis shows a distribution of size classes in nanometers, while the y-axis shows the relative intensity of the scattered light.

Fluorescence transients were measured and fitted by using a commercially available spectrophotometer (LifeSpec-ps) from Edinburgh Instrument (excitation wavelength 409 nm and 80 ps instrument response function (IRF)) with an attachment for temperature-dependent studies (Julabo, Model F32). The details of time-resolved measurements can be found elsewhere.[57] The time-dependent fluorescence Stoke's shifts, as estimated from TRES, were used to construct the normalized spectral shift correlation function or the solvent correlation function $C(t)$ defined as

$$C(t) = \frac{\nu(t) - \nu(\infty)}{\nu(0) - \nu(\infty)} \tag{2}$$

where $\nu(0)$, $\nu(t)$, and $\nu(\infty)$ are the emission maximum (in cm⁻¹) at time zero, t, and infinity, respectively. The $\nu(\infty)$ values had been taken to be the emission frequency beyond which an insignificant or no spectral shift was observed. The $C(t)$ function represents the temporal response of the solvent relaxation process as it occurs around the probe following its photoexcitation and the associated change in the dipole moment. For anisotropy ($r(t)$) measurements, the emission polarization was adjusted to be parallel or perpendicular to that of the excitation, and anisotropy is defined as

$$r(t) = \frac{[I_{para} - GI_{perp}]}{[I_{para} + 2GI_{perp}]} \tag{3}$$
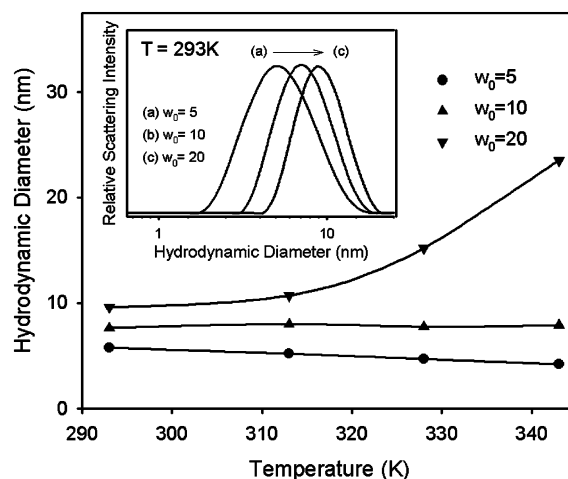

Figure 1. Hydrodynamic diameters of AOT/isooctane reverse micelles of different hydrations (w_0) as a function of temperature. Solid lines are guide to eyes. Typical DLS signals for different RM systems at 293 K are presented in the inset.

where G, the grating factor, was determined following a longtime tail matching technique.[64] All the anisotropies were measured at the emission maxima.

Results and Discussion

Figure 1 depicts the hydrodynamic diameter (d_h) of the RMs of various w_0 values at different temperatures as obtained from DLS measurements. As evident from the inset of Figure 1, the RMs are essentially monodisperse in nature. The diameter of the RMs increases with increasing w_0 value. This finding is in accordance with the previous DLS measurements reported from our group.[65] From the temperature-dependent DLS measurements, it is evident that temperature has a little or insignificant effect on the $w_0 = 5$ and 10 RMs. However, with the $w_0 = 20$ RM, the micelle grows in size with an increase in temperature, and d_h increases from 9.6 to 23.5 nm when the temperature is increased from 293 to 343 K (Figure S1 in the Supporting Information). It can be noted that for percolating RM systems, the size of the RMs increases in the vicinity of the percolation threshold temperature due to the coalescence of droplets.[66] Such droplet fusion in RMs depends upon different physicochemical conditions such as the nature of the oil (aliphatic, aromatic, and hydrophilic), surfactant, temperature, etc. To coalesce, the surfactant monolayer of a RM should be fluid, and a region of positive curvature must be generated in it.[67] Interfacial fluidity increases with increasing water loading (w_0) and/or temperature for the interacting RMs. AOT/i-Oc RM systems are prone to such kinds of droplet coagulation.[68] In the present case, the temperature-induced increase in the droplet size of the $w_0 = 20$ RM is a signature of the onset of such a process. For the other two systems, the non-interacting hard sphere nature of the droplets prevails at all the studied temperatures as the sizes of these RMs do not change with temperature. Thus, the DLS study confirms the structural integrity of the $w_0 = 5$ and 10 RM systems and an increase in the size of the $w_0 = 20$ system with respect to temperature.

(64) O'Connor, D. V.; Philips, D. *Time Correlated Single Photon Counting*; Academic Press: London, 1984.

(65) Shaw, A. K.; Pal, S. K. *J. Phys. Chem. B* **2007**, *111*, 4189−4199.

(66) Moulik, S. P.; De, G. C.; Bhowmik, B. B.; Panda, A. K. *J. Phys. Chem. B* **1999**, *103*, 7122−7129.

(67) Fletcher, P. D. I.; Howe, A. M.; Robinson, B. H. *J. Chem. Soc., Faraday Trans. 1* **1987**, *83*, 985−1006.

(68) Paul, B. K.; Mitra, R. K.; Moulik, S. P. In *Encyclopedia of Surface and Colloid Science*; Somasundaran, P., Ed.; Taylor and Francis Books: New York, 2006; pp 3927−3956.
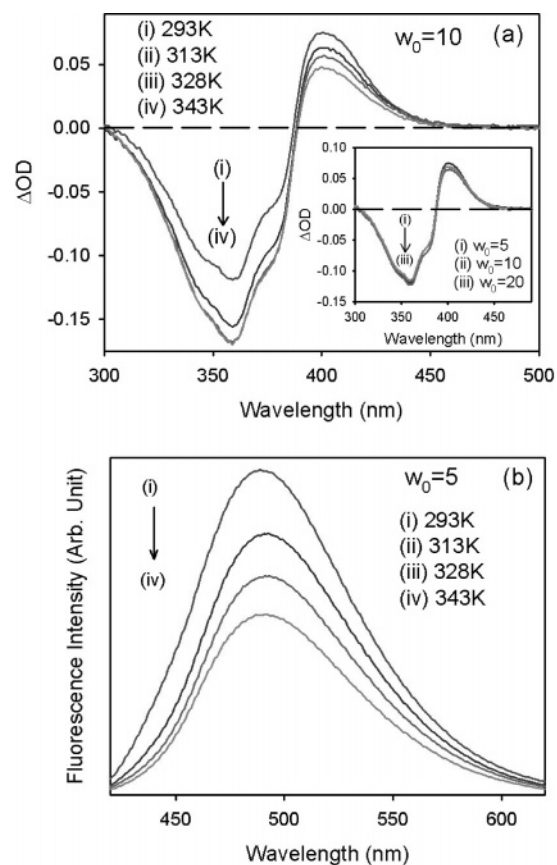
Figure 2. (a) Difference absorption spectra of C-500 in AOT/isooctane reverse micelles (with respect to C-500 in i-Oc) with w_0 = 10 at different temperatures. Difference absorption spectra of C-500 in AOT/isooctane reverse micelles with w_0 = 5, 10, and 20 at 293 K is presented in the inset. (b) Emission spectra of C-500 in AOT/isooctane reverse micelles with w_0 = 5 at different temperatures.

Figure 2a depicts the difference absorption spectra of C-500 in AOT/i-Oc RM of different w_0 values at 293 K (inset of Figure 2a) and with w_0 = 10 at different temperatures, in which the absorption spectrum of C-500 in i-Oc has been subtracted from that of C-500 in AOT/i-Oc RM. A representative absorption spectra of C-500 in AOT/i-Oc RM with w_0 = 10 at different temperatures has been provided in the Supporting Information (Figure S2). As evidenced from the figure, a single absorption peak at ~400 nm was obtained for all three RM systems. The appearance of the peak at ~400 nm, which is close to that of the probe in bulk water, signifies the absorption by the C-500 molecules present at the polar AOT/i-Oc interface.[39] The spectral feature and peak position does not change with temperature, indicating that no ground state phenomenon is associated at elevated temperatures. The temperature-dependent emission spectra of C-500 in AOT/i-Oc RM excited at 409 nm at different w_0 values and different temperatures have been determined, and one such representative illustration for w_0 = 5 at 293, 313, 328, and 343 K is presented in Figure 2b. The corresponding emission peaks (λ_{max}) of the fluorescence spectra are presented in Table 1. Insignificant spectral changes of C-500 in RMs with various w_0 values as evidenced from the inset of Figure 2b indicate that the absorption spectrum reaches an equilibrium position even in RMs with the lowest hydration (w_0 = 5). It has been reported earlier that upon excitation at ~400 nm, the C-500 molecules residing at the interface selectively become excited.[39] Thus, these emission spectra report a microenvironment of the interface and its immediate polar vicinity. As evidenced from Table 1, w_0 = 5 RM produces an emission peak of 490 nm at 293 K, which

Table 1. Solvation Correlation Data for C-500 in AOT/i-Oc RM at Different w_0 and Temperature Values[a]

temp (K)	fluorescence peak (nm)	a_1	τ_1 (ns)	a_2	τ_2 (ns)	$\langle\tau_s\rangle$ (ns)	f_r	$\langle\tau_s\rangle^{corr}$ (ns)
			$w_0 = 5$					
293	490	0.31	0.11	0.67	1.72	1.18	0.73	0.86
313	493	0.46	0.25	0.52	1.30	0.79	0.70	0.55
328	493	0.49	0.21	0.48	1.21	0.68	0.66	0.45
343	493	0.44	0.16	0.54	1.03	0.63	0.59	0.37
			$w_0 = 10$					
293	495	0.55	0.42	0.44	1.34	0.82	0.68	0.55
313	497	0.77	0.29	0.23	1.06	0.47	0.64	0.30
328	496	0.73	0.17	0.27	0.90	0.37	0.57	0.21
343	496	0.64	0.16	0.35	0.55	0.33	0.48	0.16
			$w_0 = 20$					
293	498	0.48	0.22	0.51	0.86	0.54	0.61	0.33
313	499	0.77	0.21	0.22	0.73	0.32	0.56	0.18
328	499	0.78	0.15	0.22	0.60	0.25	0.52	0.13
343	498	0.85	0.15	0.15	0.70	0.23	0.39	0.09

[a] τ represents the solvent correlation time constant, a represents its relative weight, and f_r represents the fraction of Stokes shift recovered from our experimental setup.

suffers an ~3 nm red shift when the temperature is increased to 343 K. For the w_0 = 10 and 20 systems, the emission maxima are obtained at 495 and 498 nm, respectively, and remain unchanged upon an increase in temperature. The progressive red shift of the emission peak with increasing w_0 signifies that the probe senses a more polar environment at higher hydration. According to the static spectroscopic studies of Wong et al.,[69,70] the polarity of the water pool increases as the micellar radius increases. They attributed this increased polarity to an increase in the number of bulk-type water molecules in the water pool. The peak shift is significantly small for w_0 = 10 and 20 RMs. Water present in the small RM (w_0 = 5) hydrates the surfactant head groups. With a progressive loading of water, bulk-type water begins to form, and any further addition of water increases the water pool size by increasing the amount of bulk-type water. Calorimetric studies[12,13] suggest that beyond w_0 = 10, any further loading of water is identified as bulk-type. Also, the studies of Belletête et al.[71] confirm that the effective dielectric constant at the water/surfactant interface increases as w_0 increases reaching a plateau at w_0 = 12. The micropolarity experiments of Correa et al.[72] reveal an increase in the polarity of RM-entrapped water up to w_0 = 10 to reach a plateau.

Our present steady-state emission spectra also confirm this fact that the interface can hardly differentiate the water polarity beyond w_0 = 10. It should be noted that the dye C-500 is sparingly soluble in water and produces an emission peak at ~515 nm in water, which is in close proximity to the emission peaks obtained for w_0 = 10 and 20 systems, indicating the bulk-like nature of the water present in the pool. It should be mentioned here that absorption and emission spectra of the probe C-500 in water do not depend on the temperature. A small (~3 nm) red shift is noted for the w_0 = 5 system, and it can be argued that at a low hydration limit (w_0), water molecules present within the RM are essentially hydrating the polar head groups by making hydrogen bonds. With an increase in temperature, these partially im-

(69) Wong, M.; Thomas, J. K.; Nowak, T. *J. Am. Chem. Soc.* **1977**, *99*, 4730–4736.

(70) Wong, M.; Thomas, J. K.; Graetzel, M. *J. Am. Chem. Soc.* **1976**, *98*, 2391–2397.

(71) Belletête, M.; Lachapelle, M.; Durocher, G. *J. Phys. Chem.* **1990**, *94*, 7642–7648.

(72) Correa, N. M.; Biasutti, M. A.; Silber, J. J. *J. Colloid Interface Sci.* **1995**, *172*, 71–76.
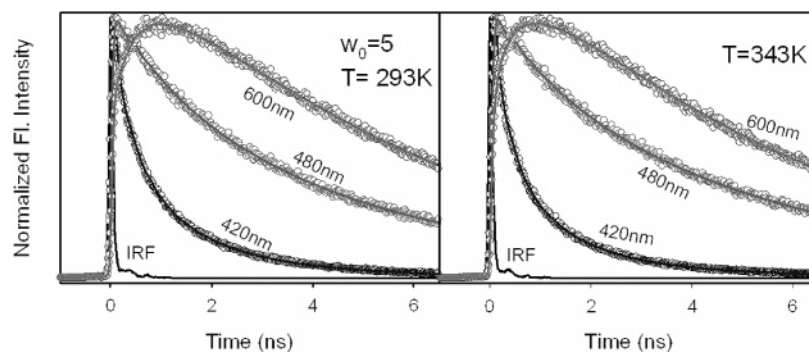
Figure 3. Fluorescence decay transients of C-500 in AOT/isooctane reverse micelles with $w_0 = 5$ at 293 and 343 K.

mobilized water molecules become free (due to the weakening of the hydrogen bonds with interface), and the probe senses a more polar environment, producing a red shift of the peak position. It should be noted that the fluorescence intensity of C-500 decreases with increasing temperature for all RM systems. It can be argued that the quantum yield of the probe increases when introduced in a restricted environment of RMs as compared to that in the bulk water. As the temperature increases, the surface-bound water in the RMs becomes converted into bulk-type, which might in turn decrease the quantum yield of the probe resulting in a decrease in the fluorescence intensity. Thus, the steady-state fluorescence measurement concludes that the emission maximum suffers a red shift for the $w_0 = 5$ system, whereas for the other two systems, the peak position does not change with temperature. The probe senses an almost similar (bulk-like) polar microenvironment when a water pool is formed irrespective of whether the RM retains its structural integrity ($w_0 = 10$) or not ($w_0 = 20$).

In an early study, the probe C-500 has been demonstrated to be a potential reporter of the solvation dynamics in the AOT/i-Oc system at room temperature.[39] Here, we study the solvation dynamics of the probe in AOT/i-Oc RM at different levels of hydration (w_0) and temperature. Figure 3 shows the fluorescence decay transients of C-500 in a $w_0 = 5$ RM system at 293 and 343 K at three selected wavelengths of 420, 480, and 600 nm. It is evidenced from Figure 3 that the decay pattern is strongly wavelength dependent. At 293 K, the blue end decays with the fitted triexponential time constants of 0.25 ns (58%), 1.1 ns (31%), and 3.0 ns (11%). The transients become slower with increasing wavelength. For the extreme red wavelength (600 nm), a distinct rise component of 1.2 ns with a negative pre-exponential value is produced along with a decay component of 5.3 ns. As the temperature is increased to 343 K, the transients still show wavelength dependency with a decrease in the time constants. Such faster decay transients with increasing temperature indicate the increased mobility of the solvating species at elevated temperatures. The decay transients of the $w_0 = 10$ and 20 systems are presented in the Supporting Information (Figure S3). As evidenced from the figures, with an increase in w_0, the transients at a particular wavelength become faster. This observation is attributed to the increased solvent mobility as the micellar interior expands.[1,10,73] As w_0 increases, the core water pool grows, leaving proportionately less water bound to the micellar interface.

A representative TRES for C-500 in AOT/RMs at 293 K with $w_0 = 5$ is presented in Figure 4a. It can be seen that the emission peak undergoes red shift with time. The $C(t)$ curves are obtained for all the systems at four different temperatures and are presented in Figure 4b−d. All the curves are fitted with biexponential functions, and the fitting parameters are presented in Table 1.

A representative figure showing the time dependence of the transient frequency maximum for the $w_0 = 10$ system at 293 K is depicted in the Supporting Information (Figure S4). Some of the curves provide better χ^2 values when fitted with triexponential functions, but the average solvation time $\langle \tau_s \rangle$, expressed as $\langle \tau_s \rangle = \sum_i a_i \tau_i$, does not change appreciably by a triexponential fitting. Thus, we prefer to fit the curves with biexponential functions. It could be noted that the subpicosecond component, which is due to solvation of the probe by the bulk water, is missed by our instrumental resolution. The solvation obtained in the present study is broadly due to the bound water molecules (with different strengths of hydrogen bonding interactions) present in the RM. In this regard, one could average out the slow and fast components, which in turn are both slower as compared to the bulk water solvation. It is evidenced from Table 1 that one component is of the order of several hundreds of picoseconds, while the other is of the order of a few nanoseconds. The time constants are consistent with the reported[30] results on C-480 in AOT/i-Oc RMs. Such slow time components have recently been reported from our group using a water soluble dye acridine orange (AO) in AOT/i-Oc RM.[65] It could be noted that Riter et al.[24] reported the ultrafast component (of the order of several hundreds of femtoseconds to a few picoseconds) of C-343 in AOT/i-Oc RM. They found that such a fast component was missing in a relatively dry RM ($w_0 = 1.1$) and increases progressively with increasing hydration. At very high hydration, the ultrafast solvation is essentially governed by the hundreds of femtoseconds component, which is identical to the solvation of the probe C-343 by water as reported by Jimenez et al.[74] Because of our limited instrument resolution (IRF = ∼80 ps), we miss such an ultrafast component, especially at elevated temperatures. As evidenced from Table 1, the $\langle \tau_s \rangle$ value is 1.18 ns for the $w_0 = 5$ system at 293 K and with an increase in temperature, it decreases: first rapidly and then moderately up to 343 K. Such a trend is more prominent for the $w_0 = 10$ and 20 systems. This observation is supported by our steady-state experiments, wherein only a marginal red shift of λ_{max} occurs with an increase in temperature (Table 1). It could also be noted that in this system, a significant part of solvation, which is due to the fast moving bulk-like water molecules, is missed by the present experimental setup, which might cause the apparent solvation saturation. The $\langle \tau_s \rangle$ value obtained for $w_0 = 10$ at 293 K in the present study is in good agreement with that reported by Majumder et al.[39] for the same RM system at room temperature. The overall decrease of $\langle \tau_s \rangle$ on increasing temperature for all three systems indicates that an increase in temperature accelerates the solvation process at the interface irrespective of the water pool size. Numerous experimental evidence indicates that even in a large water pool ($w_0 \geq 10$), the properties of the

(73) Cho, C. H.; Chung, M.; Lee, J.; Nguyen, T.; Singh, S.; Vedamuthu, M.; Yao, S.; Zhu, J.-B.; Robinson, G. W. *J. Phys. Chem.* **1995**, *99*, 7806−7812.

(74) Jimenez, R.; Fleming, G. R.; Kumar, P. V.; Maroncelli, M. *Nature (London, U.K.)* **1994**, *369*, 471−473.
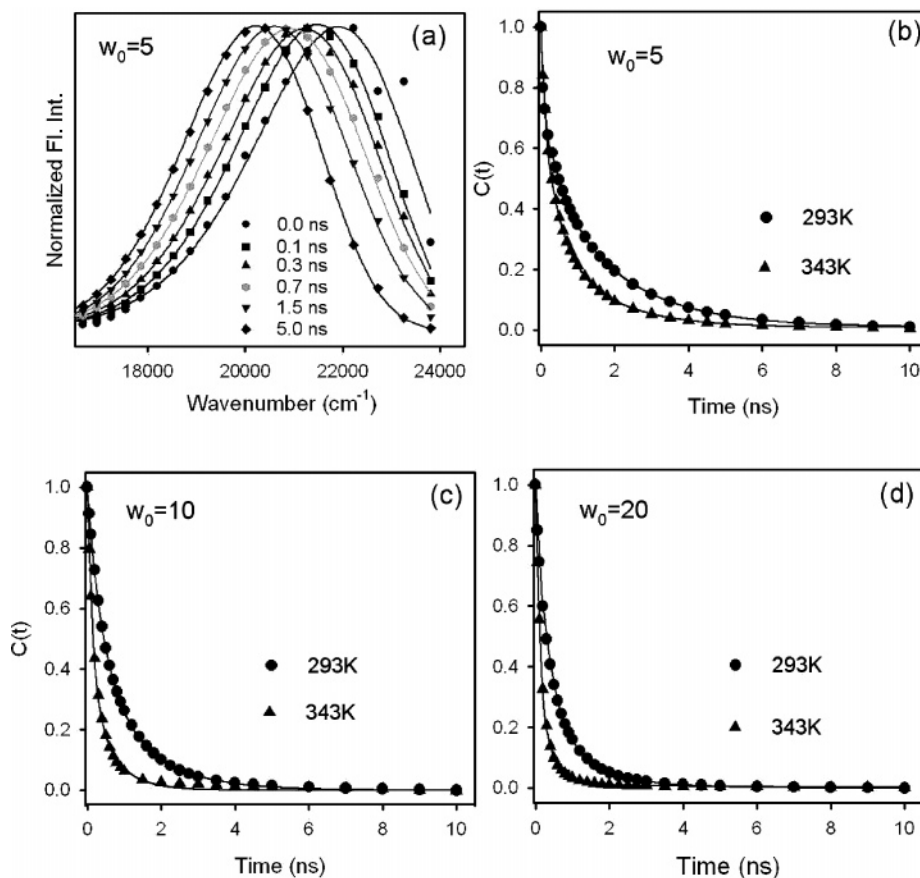
Figure 4. (a) Time-resolved emission spectra (TRES) for $w_0 = 5$ RM at 293 K. (b–d) Solvation correlation function, $C(t)$, of C-500 in AOT/isooctane reverse micelles with $w_0 = 5$ (b), 10 (c), and 20 (d) at 293 and 343 K.

confined water differ from those of the bulk water.[75–77] Thus, almost bulk-like behavior of the water inside the pool is not expected even at higher w_0 values. The observed slow timescales (in the order of a few nanoseconds) of the present system are due to the slow moving interfacially bound water molecules that become faster upon an increase in temperature.

As mentioned earlier, we miss a considerable fraction of Stokes shift due to our limited instrumental resolution, and we determined the loss in the dynamic Stokes shift using the procedure developed by Fee and Maroncelli,[78] where $\nu(0)$ can be calculated by the following equation:

$$\nu^p_{em}(0) = \nu^p_{abs} - [\nu^{np}_{abs} - \nu^{np}_{em}] \tag{4}$$

where ν^p_{abs}, ν^{np}_{abs}, and ν^{np}_{em} are the absorption peak in polar solvent, absorption peak in nonpolar solvent, and emission peak in nonpolar solvent, respectively. In the present study, we use cyclohexane as the nonpolar solvent with absorption and emission maxima of C-500 at 360 and 410 nm, respectively. Water is used as the polar solvent in which C-500 produces an absorption peak at 390 nm. We calculate a 27% loss in the dynamical Stokes shift for $w_0 = 5$ at 293 K. The loss is 41% at 343 K. For the more hydrated systems, the loss is higher, and for $w_0 = 20$, the loss is 39% at 293 K and 61% at 343 K. The fraction of Stokes shift recovered from our experimental setup (f_r) (i.e., the ratio of $\Delta\nu$ ($\nu(0) - \nu(\infty)$), obtained by using $\nu(0)$ to that obtained by using

$\nu^p_{em}(0)$ using eq 4) is presented in Table 1 for all the systems. Sen et al.[34] previously reported a 31% loss in Stokes shift using 2,6-toluidinonapthalene sulfonate (TNS) in AOT/heptane RM with $w_0 = 56$ at room temperature. Since the contribution of the subpicosecond component of the solvation dynamics to the average solvation times is very small, the corrected solvation time ($\langle \tau_s \rangle^{corr}$) is given by[79]

$$\langle \tau_s \rangle^{corr} \sim f_r \langle \tau_s \rangle \tag{5}$$

We calculate $\langle \tau_s \rangle^{corr}$ for all the systems, and these data are presented in Table 1. It should be noted that the possibility of ground state hydrogen bonding of the probe with the solvent might affect the observed Stoke's shift. To understand this possibility, we carried out photophysical studies of the dye in two polar aprotic solvents, namely, acetonitrile and dioxane. The fluorescence decay lifetime of C-500 in these two solvents closely resembles that in water. Thus, such a possibility and a consequent effect on the solvation dynamics could be overruled.

The observed temperature-induced acceleration of solvation dynamics in AOT/i-Oc RM must be associated with the bound-to free-type transition of water molecules with temperature, which in turn is governed by an Arrhenius type of activation energy barrier crossing model.[54,57,80] We fit an Arrhenius plot using the $\langle \tau_s \rangle^{corr}$ values listed in Table 1 for all three systems, and the result is depicted in Figure 5. As evidenced from Figure 5, all three systems exhibit a good linear fit, and the estimated E_a values are 3.4 ± 0.3, 4.9 ± 0.5, and 5.1 ± 0.5 kcal mol^{-1} for $w_0 = 5$, 10, and 20 systems, respectively. The 3.4 kcal mol^{-1} value obtained

(75) Amararene, A.; Gindre, M.; Le, Huerou, J.-Y.; Nicot, C.; Urbach, W.; Waks, M. *J. Phys. Chem. B* **1997**, *101*, 10751–10756.

(76) D'Angelo, M.; Fioretto, D.; Onori, G.; Palmieri, L.; Santucci, A. *Phys. Rev. E* **1996**, *54*, 993–996.

(77) Carlstroem, G.; Halle, B. *Langmuir* **1988**, *4*, 1346–1352.

(78) Fee, R. S.; Maroncelli, M. *Chem. Phys.* **1994**, *183*, 235–247.

(79) Roy, D.; Mondal, S. K.; Sahu, K.; Ghosh, S.; Sen, P.; Bhattacharyya, K. *J. Phys. Chem. A* **2005**, *109*, 7359–7364.

(80) Nandi, N.; Bagchi, B. *J. Phys. Chem. B* **1997**, *101*, 10954–10961.
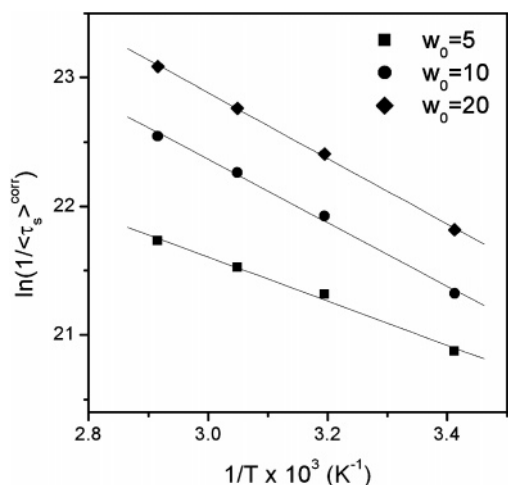
Figure 5. $\ln(1/\langle\tau_s\rangle^{corr})$ against $1/T$ plot for AOT/i-Oc RM with w_0 = 5, 10, and 20. Straight lines are linear fits.

for the $w_0 = 5$ system is in good agreement with that obtained for the interfacial water transition process in SDS micelles.[57] It should be noted that at $w_0 = 5$, the water molecules present in AOT/i-Oc RM is essentially of interfacial type and that a temperature-induced transition between the different kinds of water present at the surfactant interface is associated with an energy barrier of 2.4–4 kcal mol^{-1}.[81] For the hydrated systems ($w_0 \geq 10$), wherein the RM waterpool is formed, the transition is bound to the bulk-type, which is associated with a higher energy barrier (7–8 kcal mol^{-1}). In the present study, we found an E_a value of ~5 kcal mol^{-1}, which might be due to an averaged effect as a significant fraction of the dye molecules is still associated with the interface even at elevated temperatures. It could also be noted that the E_a values are identical for $w_0 = 10$ and 20. As observed from the steady-state experiments, the probe can hardly differentiate the water type in these two RMs producing identical E_a values. The DLS study reveals that for the $w_0 = 20$ system, the micellar size increases with an increase in temperature. This implies an increase in the radius of curvature of the AOT interfacial monolayer and a corresponding decrease in the rigidity of the film. But, the similar effect of temperature on the solvation dynamics of this system with that of the $w_0 = 10$ system and identical E_a values indicates that the mechanical properties of the interfacial monolayer has no or an insignificant effect on the observed solvation dynamics. A detailed study into this aspect, including interacting and non-interacting RM droplet systems, would be of much interest and is underway in our laboratory.

We measured the temporal anisotropy decay, $r(t)$, of the probe in AOT/i-Oc RMs at different w_0 values and temperatures, and a representative diagram for the $w_0 = 5$ system at 293 and 343 K is presented in Figure 6a. The rotational correlation time constants are given in Table 2. It can be observed from Table 2 that the slower component decreases with increasing w_0 values at constant temperature, which is identical to that reported by Shaw and Pal[65] for the AO in the AOT/i-Oc RM system. The time constants obtained for the $w_0 = 10$ system at 293 K are in good agreement with those reported by Majumder et al.[39] for the same system at room temperature. It can also be noted that the time constant of the slower component decreases with increasing temperature for all the studied systems. This certainly indicates that the probe is more free to move in larger micelles and at elevated temperatures. To understand the effect of temperature on the rotational relaxation process of the probe inside the RM
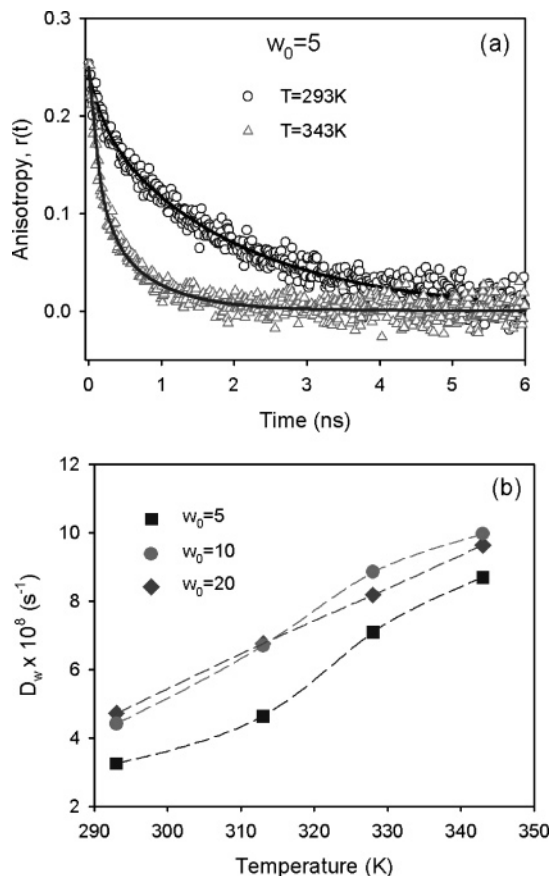

Figure 6. (a) Time-resolved anisotropy decay, $r(t)$, of C-500 in AOT/isooctane reverse micelles with $w_0 = 5$ at 293 and 343 K. (b) Diffusion coefficient for wobbling motion (D_w) of C-500 in AOT/isooctane reverse micelles at different temperatures. Dotted lines are guide to eyes.

Table 2. Fluorescence Anisotropy Decays ($r(t)$) and Wobbling-in-Cone Data of C-500 in AOT/i-Oc RM at Different w_0 and Temperature Values[a]

temp (K)	r_0	τ_{fast} (ns)	τ_{slow} (ns)	θ_w (deg)	$D_w \times 10^8$ (s^{-1})
		$w_0 = 5$			
293	0.26	0.20 (35%)	1.70 (65%)	30.15	3.256
313	0.25	0.18 (45%)	1.26 (55%)	35.26	4.641
328	0.24	0.13 (49%)	0.92 (51%)	37.29	7.091
343	0.24	0.12 (54%)	0.72 (44%)	40.92	8.700
		$w_0 = 10$			
293	0.27	0.18 (43%)	1.27 (57%)	34.24	4.416
313	0.26	0.13 (48%)	0.77 (52%)	36.79	6.705
328	0.24	0.11 (54%)	0.58 (46%)	39.87	8.846
343	0.24	0.11 (63%)	0.46 (37%)	44.68	9.968
		$w_0 = 20$			
293	0.26	0.18 (46%)	1.20 (54%)	35.77	4.718
313	0.27	0.13 (50%)	0.65 (50%)	37.81	6.761
328	0.25	0.11 (53%)	0.47 (47%)	39.35	8.182
343	0.24	0.11 (62%)	0.44 (38%)	44.13	9.638

[a] Numbers in parentheses of τ_{fast} and τ_{slow} columns signify the relative percentage of the components in the total anisotropy.

nanopool in a more quantitative manner, the biexponential anisotropy decay was analyzed using the two-step and wobbling-in-cone model.[82–85] Assuming that the slow and fast motion are separable, the slow (τ_{slow}) and fast (τ_{fast}) rotational time constants

(81) Pal, S.; Balasubramaian, S.; Bagchi, B. *J. Phys. Chem. B* **2003**, *107*, 5194–5202.

(82) Lipari, G.; Szabo, A. *J. Chem. Phys.* **1981**, *75*, 2971–2976.
(83) Lipari, G.; Szabo, A. *J. Am. Chem. Soc.* **1982**, *104*, 4546–4559.
(84) Lipari, G.; Szabo, A. *Biophys. J.* **1980**, *30*, 489–506.
(85) Wang, C. C.; Pecora, R. *J. Chem. Phys.* **1980**, *72*, 5333–5340.

can be related as

$$\frac{1}{\tau_{slow}} = \frac{1}{\tau_l} + \frac{1}{\tau_m} \qquad (6)$$

$$\frac{1}{\tau_{fast}} = \frac{1}{\tau_w} + \frac{1}{\tau_{slow}} \qquad (7)$$

where, τ_l and τ_w are the time constants for the lateral diffusion and the wobbling motion of the probe, respectively. τ_m is the time constant for the overall rotation of the RM and is given by the Stokes−Einstein−Debye equation

$$\tau_m = \frac{\eta V_h}{k_b T} \qquad (8)$$

where, V_h is the hydrodynamic volume of RM and η is the viscosity of the dispersing solvent. It could be noted that τ_m values are an order of magnitude higher than the τ_{fast} and τ_{slow} values. Hence, the overall rotation of the RM does not contribute to the decay of the anisotropy. In view of this, τ_{fast} and τ_{slow} essentially represent the time constants for wobbling motion and lateral diffusion, respectively.

According to this model, the rotational anisotropy decay function is denoted as

$$r(t) = r_0[\beta e^{-t/\tau_{slow}} + (1 - \beta)e^{-t/\tau_{fast}}] \qquad (9)$$

where $\beta = S^2$ and S is the generalized order parameter that describes the degree of restriction on the wobbling-in-cone orientational motion. Its magnitude is considered as a measure of the spatial restriction of the probe and can have a value from zero (for unrestricted rotation of the probe) to 1 (for completely restricted motion). The semicone angle θ_w is related to the ordered parameter as

$$S = \frac{1}{2}\cos\theta_w(1 + \cos\theta_w) \qquad (10)$$

The diffusion coefficient for wobbling motion D_w can be obtained from the following relation

$$D_w = \frac{1}{(1 - S^2)\tau_w}\left[\frac{x^2(1 + x)^2}{2(x - 1)}\left\{\ln\left(\frac{1 + x}{2}\right) + \frac{1 - x}{2}\right\} + \frac{1 - x}{24}(6 + 8x - x^2 - 12x^3 - 7x^4)\right] \qquad (11)$$

where $x = \cos\theta_w$. The results obtained from the analysis are summarized in Table 2 and Figure 6b. It can be observed that the wobbling cone angle (θ_w) for all the systems increases with increasing temperature. The diffusion coefficient (D_w) values are of the same order of magnitude as reported by Shaw and Pal[65] for AO in AOT/i-Oc RM and increases with increasing temperature for all the systems (Figure 6b). This signifies that with increasing temperature, the probe experiences less restricted rotation in the micelle. This might be due to the faster movement of the trapped water at elevated temperatures and/or diffusion

of the probe toward central bulk-type water of the RMs. It can be seen from the table that the θ_w and D_w values are comparable in $w_0 = 10$ and 20 systems at all temperatures. Thus, the probe experiences a similar kind of microenvironment in these two systems, which corroborates well with the steady-state and solvation dynamics results.

It should be noted from Tables 1 and 2 that the average solvation time constant $\langle\tau_s\rangle$ and average rotational time constant $\langle\tau_r\rangle$ decrease with an increase in temperature for all the RM systems (Figure S5 in the Supporting Information). Thus, the change in microviscosity at the micellar interface might have caused the observed temperature-induced change in the solvation dynamics. The diffusion coefficient for wobbling motion (D_w) of the probe increases with an increase in temperature (Table 2). Such an increase in D_w is associated with a decrease in the microviscosity at the micellar interface,[86,87] which corroborates to the conversion of surface bound water to free water.[80,81,88] This change causes the observed faster solvation dynamics at elevated temperatures, and the calculated E_a value corroborates with the transition of surface-bound to free-type water molecules, which consequently decreases the microviscosity at the interface.

Conclusion

Our studies explored the temperature-dependent dynamics of solvation of a probe, C-500, at the polar surfaces of AOT/isooctane RMs with various degrees of hydration (w_0). The nature of temperature-dependent structural changes of the RMs with various sizes has also been explored by using DLS studies. Our studies have confirmed that for all the RMs, the solvation dynamics of the probe become faster with an increase in temperature. We correlate the faster dynamics with the transformation of interfacially bound water into bulk water at elevated temperatures. A more quantitative picture of the transformation is revealed in an energy barrier crossing model. For the less hydrated system ($w_0 = 5$, where a definite water pool is not present), the activation energy is found to be 3.4 kcal mol^{-1}, indicating a temperature-induced interchange between the interfacial water molecules. On the other hand, for hydrated RMs ($w_0 = 10$ and 20, where a definite waterpool is present), the E_a value is higher, indicating a bound to bulk-type transition of water. The rotational anisotropy study also corroborates with this result as the probe experiences a less restricted environment at elevated temperatures. To our understanding, the temperature-dependent dynamical studies of the probe in the restricted environments of RMs are important to unravel the diffusion of entrapped water in biologically relevant environments under the influence of temperature.

Supporting Information Available: Figures (S1−S5) mentioned in the text. This material is available free of charge via the Internet at http://pubs.acs.org.

(86) Dutt, G. B. *J. Phys. Chem. B* **2003**, *107*, 10546−10551.
(87) Dutt, G. B. *J. Phys. Chem. B* **2005**, *109*, 4923−4928.
(88) Pal, S.; Balasubramaian, S.; Bagchi, B. *J. Chem. Phys.* **2002**, *117*, 2852−2859.